Available online at www.sciencedirect.com
SCIENCE DIRECT®
Journal of Power Sources 135 (2004) 332–343
JOURNAL OF POWER SOURCES
www.elsevier.com/locate/jpowsour

Comparative studies of self-discharge by potential decay and float-current measurements at C double-layer capacitor and battery electrodes

Jianjun Niu, Brian E. Conway*, Wendy G. Pell

Chemistry Department, University of Ottawa, 10 Marie Curie Street, Ottawa, Ont., Canada K1N 6N5

Received 5 February 2004; accepted 18 March 2004

Available online 17 June 2004

Abstract

Charged electrochemical capacitors and battery electrodes are in a state of high Gibbs energy in relation to that of their discharged states; hence there is a thermodynamic "driving force" for their self-discharge on open-circuit. Several mechanisms for self-discharge can be envisaged and diagnostically distinguished. They must take place by mixed cathodic/anodic electrochemical processes (as in corrosion) or, in some cases, by a surface-chemical process.

Self-discharge can be characterized by two procedures: (a) measurement of open-circuit decline of electrode potential or state-of-charge with time or (b) by establishing the polarizing currents, so-called float-currents, at various potentials in the self-discharge process that are required just to maintain those respective potentials constant. The importance, for either case, of characterizing the self-discharge behavior individually for each electrode of a cell pair (using a third electrode as a reference) is stressed.

Experimental data are presented for potentiostatic float-current measurements at porous C-cloth and glassy-C electrodes, and related to digital potential-decay measurements under the same conditions in aqueous H_2SO_4 below the decomposition potential of the solution. Treatment of an equivalent circuit model enables the time dependence of components of double-layer charging and self-discharge under potentiostatic float conditions to be understood and evaluated.

Keywords: Electrochemical capacitors; Supercapacitors; Asymmetric capacitors; Self-discharge; Float-currents; Leakage current

1. Introduction and significance of self-discharge processes

In previous papers [1,2], we analyzed the various factors determining rates of self-discharge, in time, of electrochemical charge-storage devices, as determined by the potential-decay procedure. In the charged state, batteries and supercapacitors [3,4] are in a state of higher Gibbs (free) energy, *G*, than in their discharged state so there is a thermodynamic "driving force" for spontaneous decline of *G* with time. The actual rate of this decline, manifested as diminution of cell voltage (or available charge) of the electrochemical capacitor or battery with time, is determined by the *mechanism*(*s*) of the process(es) by which the self-discharge and decline of *G* takes place, and by the temperature. The situation is not unlike that in a reaction between potentially reactive chemical compounds (high *G*) which, when mixed, proceed to produce products (lower *G*) at a rate dependent on the kinetics and mechanism of the reaction(s) involved that are dependent on concentration and temperature.

Rates of decline of voltage of an electrochemical power source, "self-discharge", are similarly determined by the mechanisms and rates of processes that can take place at the interfaces of the electrodes of the device, as influenced by the *kinetics* of the electrochemical processes involved.

Although self-discharge is always of fundamental interest in the behavior of electrochemical power sources, whether it is of practical importance or not depends on the *application of the capacitor device*. For load-leveling applications in hybrid EV power-trains [4,5] or for bridging short-term power outages, it may not be of practical significance since recharge is intermittent. In stand-alone or standby applications, where the device has to be on-line for appreciable periods of time before recharge, obviously self-discharge behavior is of major importance for device performance specifications.

On open-circuit of a charged battery or capacitor device there is no external circuit through which discharge by Faradaic passage of electronic charges can pass, as is the case for such devices operating in the regular way

* Corresponding author. Tel.: +1-613-562-5481; fax: +1-613-562-5170.
E-mail address: wpell@science.uottawa.ca (B.E. Conway).

0378-7753/$ – see front matter © 2004 Elsevier B.V. All rights reserved.
doi:10.1016/j.jpowsour.2004.03.068

through an ohmic load. Hence, open-circuit self-discharge must take place through coupled anodic and cathodic processes, passing parasitic currents at one or both individual electrodes, separately. Such processes are analogous to corrosion of metals on open-circuit where coupled half-cell electrochemical processes, anodic and cathodic, take place simultaneously at a single electrode interface at a common mixed potential ("mischpotential"), determined jointly by the kinetics of the anodic and cathodic partial processes taking place at a time-dependent common potential.

Self-discharge must proceed by an analogous mechanism involving coupled anodic and cathodic partial processes, normally of a Faradaic nature involving interfacial charge-transfer processes. Since self-discharge, by definition, involves progressive, time-dependent loss of charge, the state-of-charge (SOC) continuously diminishes with time, usually at progressively diminishing rate. It is important, as will be discussed later, to recognize that self-discharge rates at given potentials can be different at the positive and negative electrodes of a double-layer capacitor pair since specific capacitance values can differ for a given material (as is well known for Hg [6]) under positive compared with negative directions of polarization. Apart from self-discharge being usually different at the anode and cathode of a battery, or the positive and negative electrodes of a capacitor device, there can be fundamental differences in the significance of self-discharge at battery and capacitor type electrodes, for the following reasons.

Charging or discharging of battery electrodes involves principally Faradaic charge-transfer processes which change the chemical states, or state of oxidation, of the electrode materials, and are usually associated with *phase changes*. Charging or discharging of electrochemical double-layer capacitor devices, e.g. employing high-specific-area porous carbon materials as electrodes, normally involves *non-Faradaic* charge accumulations of opposite sign across the interfaces of two component electrodes (polarized in opposite directions), without phase changes. Only on overcharge to potential differences exceeding the thermodynamic decomposition potentials (ΔE_d) of the cell electrolyte does the passage of charge from the external circuit become increasingly Faradaic as cell voltage is continued to increase beyond ΔE_d.

The above differences in the charging processes in a battery-cell compared with a capacitor-cell are important for considering the nature and mechanisms of processes of self-discharge at the two systems. These differences provide the basis for some of the discussions and experimentation reported in the present paper.

2. Distinguishable mechanisms of self-discharge

Three situations arise in self-discharge phenomena that should be recognized in relation to choice of experimental design and bases of interpretation of results. They are as follows:

(a) Self-discharge at electrodes which have been polarized to overcharge potentials, i.e. beyond potentials corresponding to the thermodynamic decomposition potential of the solution. Examples are the alkaline Ni–O–OH and the acid PbO_2 cathodes. Self-discharge, in such cases, then proceeds by continuation of the Faradaic overcharge process, viz. anodic O_2 evolution, on open-circuit but coupled with a cathodic partial process, theoretically down to the reversible O_2/H_2O potential.
(b) Self-discharge by parasitic processes involving Faradaic impurity reactions (sometimes redox shuttle processes [2]) that can be cathodic or anodic, and may be diffusion-controlled. Such processes can arise at battery-type anodes or cathodes and especially in the case of double-layer-type electrochemical capacitors where impurity parasitic currents can arise.
(c) Apparent self-discharge, over relatively short times, following interruption of polarizing currents at porous-C electrodes due to non-uniformity of charge acceptance down and amongst pores. This can be experimentally observed and physically simulated in the behavior of hardware, multi-element *C*/*R* circuits, as in our Ref. [7]. Similar effects arise, but for different reasons, at RuO_2 pseudocapacitance devices owing to non-uniformity of states of oxidation (or reduction) of the RuO_2 active material in the near-surface region of such electrodes [2].
(d) A different origin of self-discharge behavior arises at some two-electrode battery configurations where products of charging or corrosion at one electrode become transferred, by diffusion, to the other electrode which then suffers time-dependent depolarization. Examples arise in the operation of, e.g., Zn/air or Al/air primary cells or rechargeable Zn/Br_2 batteries and in related ways (but not referred to as "self-discharge") in the operation of methanol fuel-cells where cross-over of MeOH to the O_2 cathode interferes with its efficient operation.
(e) Finally, a more trivial origin of self-discharge can be short-circuit leakage currents between adjacent cathodes and anodes in imperfectly sealed bipolar electrode configurations. This case gives (see below) self-discharge kinetics that are clearly distinguishable from those originating from the other situations listed above.

3. Kinetic equations for potential, *V*, as a function of time, *t*, in self-discharge

In our previous papers [1,2], we analyzed comparatively three of the above types of electrochemical mechanism, and associated respective kinetic behaviors, by which self-discharge of an electrochemical capacitor or battery could take place; a summary is given below:

(1) By a Faradaic process of self-discharge involving, e.g., reduction or oxidation of impurities such as O_2, H_2O_2, Fe^{2+}/Fe^{3+}, etc., or by a Faradaic process associated with reaction of products from overcharge, as with the nickel-oxide electrode Ni–O–OH or "NiO_2".

For this case [1–3], the self-discharge current at potential V is given by

$$i_V = -C\frac{dV}{dt} = i_0 \exp\left[\frac{V}{b}\right] \quad (1)$$

where the right-hand side is the Tafel function in exp form for the current as $f(V)$ in the self-discharge reaction. At the initial potential V_i, just upon opening the circuit, $i_V \equiv i_{V_i} = i_0 \exp[V_i/b]$ and b is the Tafel slope, $RT/\alpha F$, C is the double-layer capacitance of the electrode and i_0 the exchange current density of the rate-determining self-discharge process.

Rearranging and integrating Eq. (1) gives (cf. Ref. [8]) the time dependence of V on open-circuit as

$$V_t = -b \ln\left\{\frac{i_0}{bC}\right\} - b \ln(t+\theta) \quad (2)$$

where θ includes the integration constant of Eq. (1). Then V_t is logarithmic in $(t+\theta)$ or in t for $t \gg \theta$. In cases where C itself is $f(V)$, determined empirically from experiment (as, e.g., from Fig. 1) or is intrinsically itself an $\exp f(V)$ (pseudocapacitance case [9]), V_t will differ as $f(t+\theta)$ from that given by Eq. (2).

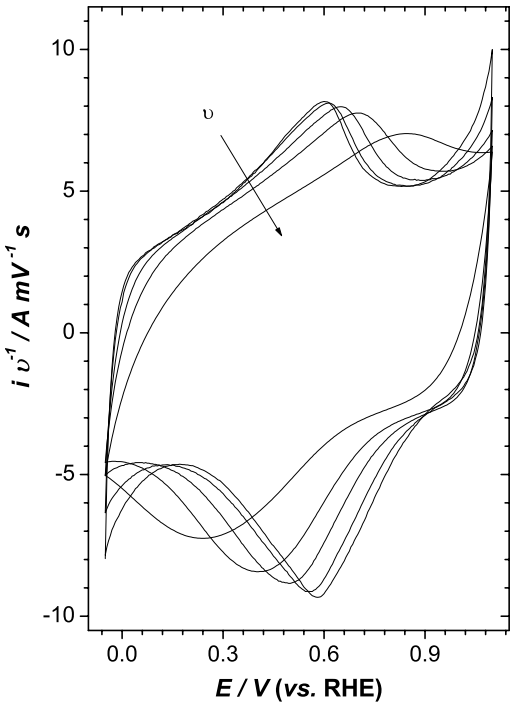

Fig. 1. Cyclic voltammograms of the Spectracarb carbon-cloth electrode in 5 M H_2SO_4 recorded for a series of sweep rates, 1–25 mV s^{-1}; arrow indicates direction of increasing sweep rate.

(2) By a diffusion-controlled Faradaic process involving depolarization by impurity reactions:

$$V_t = V_i - B\sqrt{t} \quad (3)$$

that is the self-discharge follows a *square-root relation* in time in the duration of self-discharge.

(3) Another mechanism can arise if there is "short-circuit" leakage between one electrode interface and another through a load in improperly sealed bipolar cell designs. Then, a characteristic self-discharge behavior in time arises, dependent on the magnitude of R_L, the resistance of the leakage pathway:

$$\ln\left[\frac{V_t}{V_i}\right] = -\frac{t}{R_L C} \quad (4)$$

This is easily distinguishable from the kinetics associated with Eqs. (2) and (3).

Eqs. (2)–(4) thus provide clear *diagnostic criteria* for distinguishing mechanisms of self-discharge that may characterize the time-dependent voltage of a cell on open-circuit, provided that data collection is over at least 3 decades of time [2].

A complementary approach to the use of simple, qualitatively different equivalent circuits for analysis of self-discharge kinetics, has been employment of multiple series/parallel ladder-type equivalent circuits for analysis of impedance characterization for a range of low to higher RC time constants by Miller [10], as recently applied by Dougal et al. [11].

We now proceed to treat and discuss new aspects of the self-discharge problem, as treated in terms of float-current measurements in the sections which follow.

4. Comparative evaluation of self-discharge by means of voltage decay versus "float-current" measurements

In earlier work, self-discharge was characterized by recording decline of electrode potential or cell voltage over lengthy periods of time and subjecting the data to some kind of kinetic analysis, e.g. in terms of $\log t$ plots based on Faradaic self-discharge, Eq. (2), or on some other mechanism referred to above.

More recently, a different procedure has been employed where so-called "float-currents" are recorded, i.e. the currents required just to maintain the electrode (or cell) at a given, selected constant potential in the range involved in a potential-decay experiment. This corresponds, ideally, to maintaining the electrode at a given state-of-charge (and corresponding potential) where the imposed flow of current would match the spontaneous self-discharge current that would otherwise be flowing (at a given potential) as a result of a *mixed* anodic/cathode process at the electrode's interface, as in corrosion of a base metal [12].

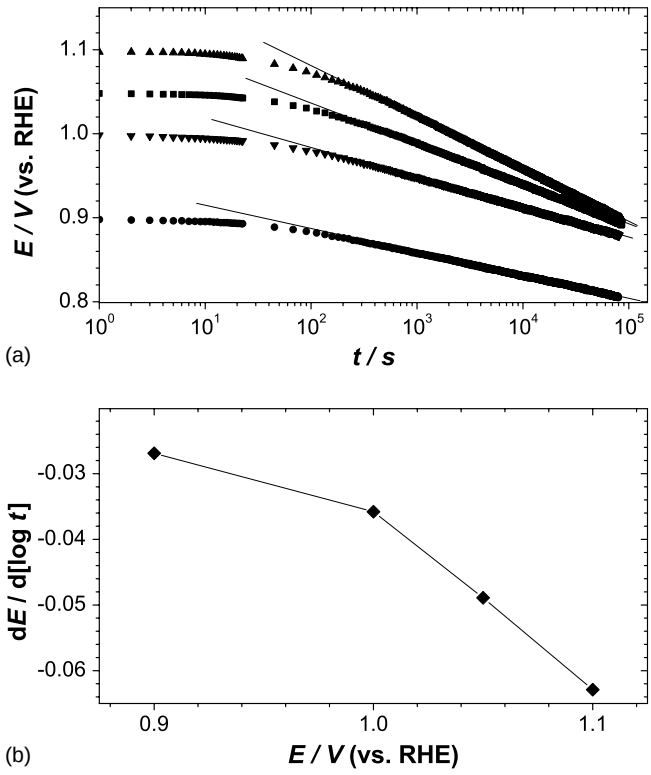

Fig. 2. (a) Potential-decay relations for self-discharge at the porous C-cloth electrode initiated at a series of declining potentials (5.0 M aq. H_2SO_4, $T = 298$ K) on positive polarization; (b) plot of the slopes of the E vs. $\log t$ relations (in (a)) as a function of the polarization potential at the C-cloth electrode.

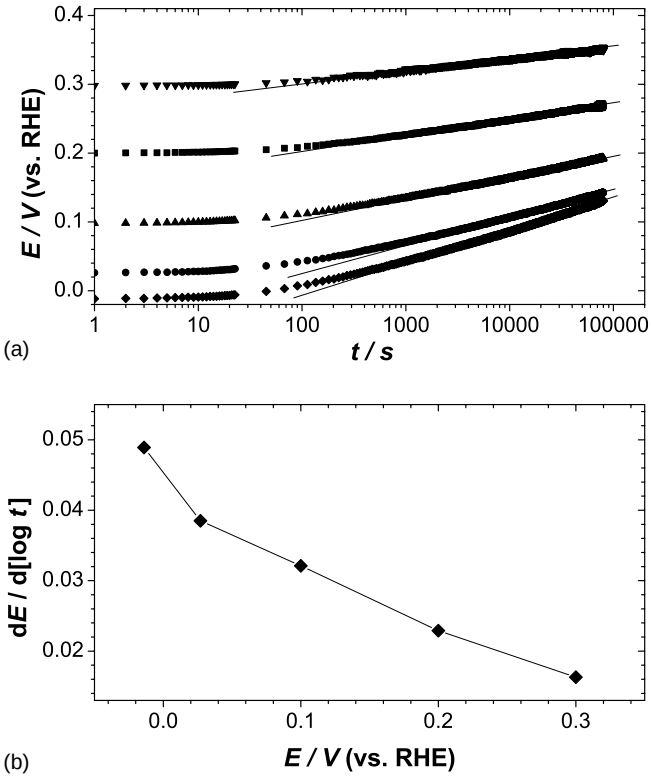

Fig. 3. (a) Potential-recovery relations at the porous C-cloth electrode initiated at a series of increasing potentials (5.0 M aq. H_2SO_4, $T = 298$ K) on negative polarization; (b) plot of the slopes of the E vs. $\log t$ relations (in (a)) as a function of the initial polarization potential at the C-cloth electrode.

In the present work, we have made such comparative measurements by means of potential-decay and float-current evaluations.

Under ideal conditions, float-currents evaluated at various potentials in the range corresponding to self-discharge decline, would remain constant in time, matching the self-discharge currents that would otherwise be passing and be dependent on potential. At the limit of interruption of a polarizing current, i.e. at the initial potential of a potential-decay curve, the self-discharge current is, in effect, the negative of the polarizing current, i, and is $-i = C(\mathrm{d}V/\mathrm{d}t)_{t=0}$ where $(\mathrm{d}V/\mathrm{d}t)_{t=0}$ is the *initial* potential decay rate [cf. Eq. (1)].

As will be shown in Section 6, the experimental behavior at the porous-C electrode differs qualitatively (see Figs. 2 and 3 later) and in a more complex way from the expected ideal behavior.

5. Experimental

Experimental procedures followed those in earlier publications [1,2,7].

Double-layer capacitor electrodes were made from "Spectracarb 2225", high-specific-area ($2500\,\mathrm{m^2\,g^{-1}}$) C-cloth material (Spectracarb Corp., Lawrence, MA) mounted at the end of a glass-tube electrode holder. Charging and self-discharge at such electrodes was followed in a three-electrode cell, i.e. using a third electrode (RHE) as a reference. Following polarization to a series of selected potentials, charging currents were interrupted and declines of electrode potential were followed by digital recording over 4–5 decades of time.

Comparative self-discharge measurements were made at a glassy-C rod electrode.

Aqueous 5.0 M H_2SO_4 was the electrolyte at 298 K. The high concentration was used in order to minimize equivalent series resistance. The porous-C electrodes were pre-filled with this electrolyte on standing.

The double-layer capacitance behavior was first characterized at various sweep-rates, υ ($\mathrm{mV\,s^{-1}}$), by cyclic voltammetry as exemplified by Fig. 1. The υ-dependence of the CVs, corresponding to dispersion of the capacitance, is due to the well known effect of distributed C and R in the porous matrix [7,13].

Analysis of potential-decay results in time was performed according to the principles explained in Ref. [2], using one or other of the Eq. (2), (3) or (4) for the purpose of comparison with results of float-current measurements made at the same electrodes (see below).

Self-discharge behavior was also examined comparatively at the C-cloth and glassy-C electrodes by means of "float-current" measurements. These were conducted by application of potentiostatic potential steps to a series of selected potentials in the range of decline of potentials that had been followed in the potential-decay measurements, with recording of the time-dependent currents arising in response to the potential steps.

The resulting current transients (see results presented below) were recorded for appreciable periods of time up to the condition where (almost) steady float-currents were attained, i.e. when the float-current reached a steady-state value equal to the self-discharge rate at the given selected potential. The basis for analysis of these current transients is given in Section 10 later.

6. Observed kinetic behavior for self-discharge at the Spectracarb C electrode

Examples of plots of V_t versus $\log t$, following interruption of currents at various values, are shown in Fig. 2. The initial curvature at small t values is expected and arises from the θ term in Eq. (2). For $t \gg \theta$, the V_t relations are almost logarithmic in t over several decades of t. However, it is seen that the negative log-slopes (Fig. 2b) of the linear regions of the plots in Fig. 2a *decrease* numerically with decreasing initial polarization potential, contrary to the expectations from Eqs. (1) and (2) (and to the behavior at Ni–O–OH, Ref. [2] and Fig. 4, later). For polarization of the C electrode in the opposite direction (i.e. for "discharge"), it is of special interest that similar potential relaxation takes place ("potential recovery"), as shown in Fig. 3, and is also approximately linear in $\log t$ when $t \gg \theta$. Note that analogous behavior was observed in our work on RuO_2 as a redox pseudocapacitance material [2].

Plots were also made (cf. Ref. [2]) of $\log[V_i/V_t]$ versus t, corresponding to leakage discharge into a load resistance. As expected for the conditions of the present experiments, such plots are not consistent with the experimental potential-decay data for a single electrode.

However, comparative experimental evaluations of self-discharge relations from small extents of overcharge of the nickel-oxide (Ni–O–OH/Ni(OH)$_2$) battery cathode, taken from various initial potentials, do converge to a common line in $\log(t + \theta)$ with increasing time, t, as t becomes $\gg \theta$, having therefore a common slope value, $-b$ (Eq. (2)), as shown for the examples in Fig. 4. This behavior of Ni oxide electrodes involves *Faradaic self-discharge*, as proven by direct measurements of O_2 evolution rates on open-circuit, contrary to the porous-C case where the self-discharge takes place *below* the solution-decomposition potential.

The behavior for the porous-C capacitor electrodes is evidently quite different from that of Ni–O–OH (Fig. 4) where

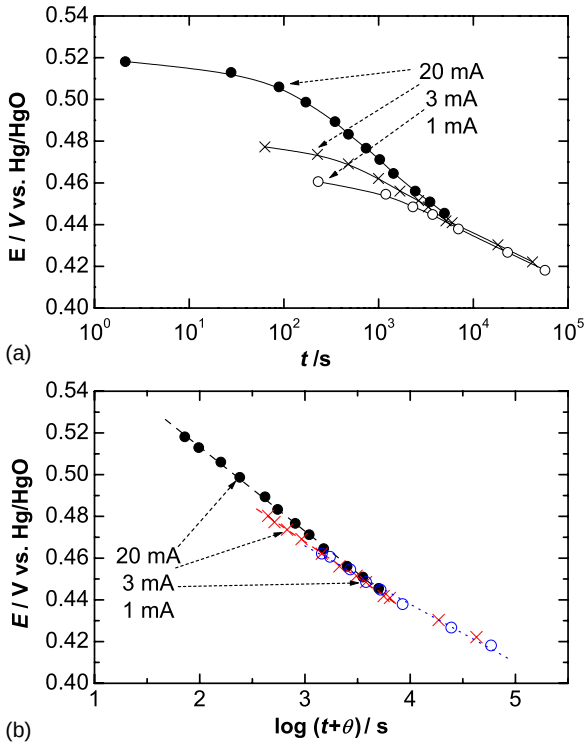

Fig. 4. Comparative potential-decay plots for self-discharge of a Ni–O–OH/Ni(OH)$_2$ battery-type electrode, following anodic polarization (charging at several rates: 20, 3 and 1 mA) in aq. KOH at 298 K. Note that decay plots from various potentials tend to a common line on $\log(t + \theta)$ plots (Eq. (2)).

the self-discharge process corresponds to (experimentally observable [8]) O_2 evolution from the Ni-oxide at overcharge potentials, i.e. above the O_2/H_2O reversible potential. The open-circuit process is Faradaic O_2 evolution coupled, as a mixed reaction, with reduction of Ni–O(>1)–OH.

Thus the open-circuit behavior of the capacitative porous-C electrodes as analyzed by $\log(t + \theta)$ plots (Figs. 2 and 3) seems fundamentally different from that for Ni–O–OH since decay from an overcharge condition is not involved in the former case. Then the question, "what is involved kinetically?", arises.

The interesting and significant feature of the potential-decay behavior of the C-cloth double-layer capacitor electrode (Figs. 2 and 3) and of glassy-C (Fig. 5) is that linear log plots in $t+\theta$ do arise, as represented by Eq. (2), but their slopes depend on the initial polarization potential (Figs. 2 and 3), and hence would not be simply identifiable as the negative of the Tafel slope of the Faradaic self-discharge reaction, Eq. (2), as applies for the nickel-oxide behaviors (Fig. 4a and b).

Proceeding in a "retro-mathematical" way to interpret the above results in terms of the exp form of Eq. (1), one would have to introduce an additional Tafel-type factor, $-b'$, leading to a compound potential dependence of self-discharge current in Eq. (1), with an overall slope of

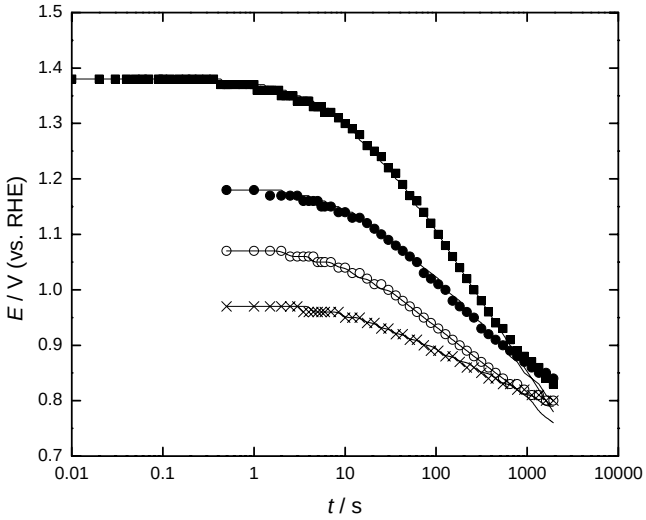

Fig. 5. Potential-decay profiles for a glassy-C electrode in 0.5 M H_2SO_4 (298 K) plotted in log t/s over seven decades of t (note that for log $t > 1$, the plots do not tend to fall on a line of common slope).

the V_t versus $\log(t + \theta)$ relation, having a value $b - b'$. To account for the observed slopes of such relations in Figs. 2 and 5, b' would have to be a function of the initial polarization potential V_i. However, it is unclear what physical significance such a factor might have, and it does not arise in self-discharge of the Ni-oxide electrode (Fig. 4).

A related way of representing the results would be to suppose that the transfer-coefficient, α, in the Tafel slope is dependent on V_i but, for each V_i, it has a different value which, however, *remains constant* over the succeeding decline of potential from that V_i. Again the origin of such behavior is obscure. A kind of "memory effect" would be required, i.e. for each V_i, a constant α applies for *further declining potential* yet α depends on the V_i at which the particular self-discharge plot was initiated.

Probably the key difference could be the time-dependent redistribution of charge in the distributed double-layer at the extended pore surfaces which arises from the de Levie "porous-electrode effect" [7,13]. Such effects have already been characterized in an earlier paper from our laboratory [7] in which potential-relaxation transients were recorded at RuO_2, following pulsed changes of electrode potential (cf. Fig. 3 and Ref. [7], referred to above). Support for such a charge-redistribution effect could be adduced from the fact that evident similar potential changes in log[time], but in the opposite direction, arise as potential-recovery, following deep discharge (Fig. 3).

Comparative potential-decay experiments were conducted at a glassy-C electrode having much lower porosity. The results are shown in Fig. 5 for self-discharge from several positive potentials. Surprisingly, the main features of the behavior are not dissimilar to those of the porous-C cloth electrode (Fig. 2), but are again different from those for the Ni-oxide electrode (Fig. 4).

7. Charge losses on self-discharge

Accompanying decline of potential on self-discharge there is, of course, a corresponding loss of charge held. This is easily calculated from the course of recorded self-discharge voltage profiles and knowledge of the electrode's capacitance, C_V, as a function of electrode potential, e.g., from CVs (not necessarily the same for a given carbon preparation at each of the two electrodes in a symmetric carbon/carbon double-layer device since the specific capacitance ($\mu F\,cm^{-2}$) of most electrode materials, e.g. Hg [6], is usually different for positive polarization (anion adsorption; greater) from that for negative (cation adsorption; less)).

The change of charge held, Δq_t, as a function of electrode potential and time on self-discharge is

$$q_i - \int_{V_i}^{V_t} C_V \,\mathrm{d}V = \Delta q_t \tag{5}$$

where q_i is the charge held initially at potential V_i, and V_t is the potential after decline over t seconds. C_V can be easily determined by means of cyclic voltammetry (Fig. 1; response current $i = C_V\,\mathrm{d}V/\mathrm{d}t$), so the integral charge loss can be quantitatively evaluated.

Often, C is almost independent of potential, V, so Δq_t can be easily evaluated, starting from various initial potentials, V_i; then Eq. (5) is simply and obviously

$$q_t = q_i - C\Delta V = (\Delta q)_t \tag{6}$$

where ΔV is the spontaneous fall of potential, $V_i - V_t$ over time t, which is directly measurable from the self-discharge profiles in time.

From the above relations, applied to *each electrode* of a cell pair, any asymmetry in $(\Delta q)_t$ (cf. Fig. 6), during self-discharge, can be evaluated and its effects on cell performance on cycling taken into account.

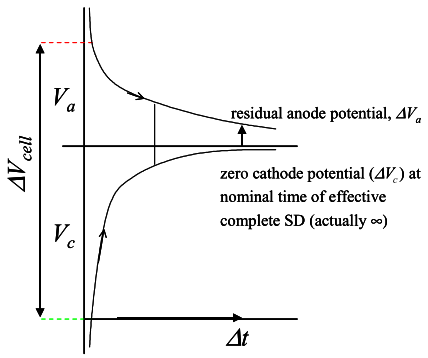

Fig. 6. Schematic comparison of asymmetry of self-discharge profiles at a capacitor and battery-type electrode in a "hybrid" electrode device.

8. Results of float-current experiments at the C-cloth electrode

Comparative float-current experiments were conducted at the C-cloth electrode in 5.0 M H_2SO_4 by means of potentiostatic polarization as explained in Section 5.

In one set of experiments, a series of potential steps were applied to the electrode potentiostatically up to, first, a series of potentials below the solvent decomposition voltage (below that for O_2 evolution) and then to several values above. The response "float-currents" that resulted were recorded in time over 3600 s, as shown in Fig. 7. Results from overcharge conditions were unsatisfactory owing to damage to the C electrode, probably due to O_2 generation in the pores with expulsion of some electrolyte from them. This could serve as a warning in practical applications where charge/discharge conditions should be carefully controlled.

Unlike the behavior expected for regular plane electrodes having small capacitance without the impediment to charging through a distributed resistance [13] (cf. Section 5), the (apparent) float-current responses, i_t, declined in time substantially (Fig. 7), eventually attaining an almost constant value which is presumably equal to the ultimately steady self-discharge rate. This situation obviously complicates the characterization of self-discharge behavior at porous electrodes using the "float-current" method, but it does give new and unexpected insights into what is occurring at porous, high-specific-area C electrodes used for electrochemical capacitor devices.

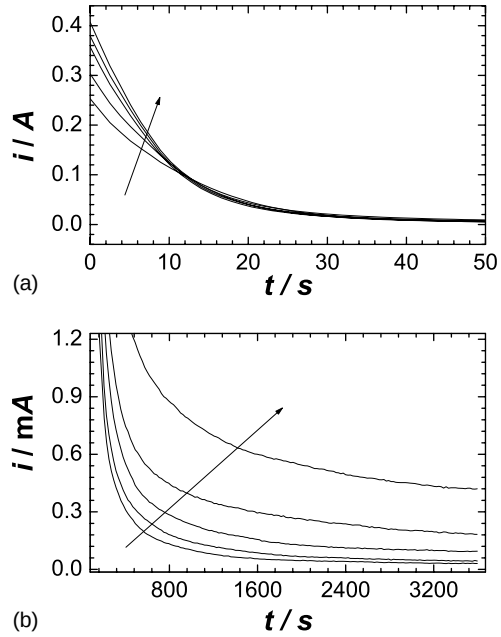

Fig. 7. Potentiostatic float-current responses recorded at the C-cloth electrode from five polarization potentials (+0.8, +0.9, +1.0, +1.05 and +1.1 V, RHE) for a duration of (a) 0–50 s and (b) 0–3600 s. Float-currents tend to the self-discharge rates at $t \rightarrow 3600$ s. Arrows show directions of increasing initial anodic polarization potentials.

These extended time-effects, we believe, are a direct result of the de Levie "porous electrode effect" [13] where a modulation voltage signal does not immediately give rise to charging of the electrode's whole double-layer capacitance due to its distributed complex "*RC*" network and large values of *C*. There is a so-called "penetration distance" [13] of the signal down pores, into the electrode matrix, depending on rise-time in voltage pulses or frequency in alternating voltage modulation.

Integration of the *i* versus *t* transients that arise from the potentiostatic polarizations at various potentials gives the charges that have to be passed cumulatively to eventually attain steady values of float-currents. Such charges correspond therefore to extents of charge that have to be passed into (or from) the porous electrode surface in order to establish a *steady state* of accommodated double-layer charge, at a given potential, associated with a *steady* self-discharge or potential-recovery current or rate.

The time-dependent float-currents, following a potential step, correspond to continuing charge adjustment at/in the porous electrode. For the case of potentiostatic charging into a capacitance in series with a resistance (Circuit 1, Section 10), in the simplest analysis, the charging current i_t as function of time would be $i_t = i_i \exp[-t/RC]$. Integration of such *t*-dependent i_t values then gives the charge delivered

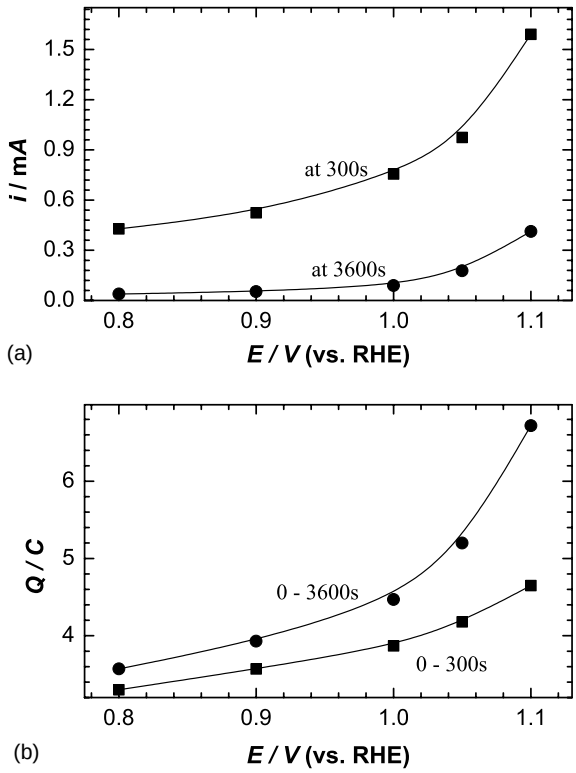

Fig. 8. (a) Current values in the transients for the C-cloth electrode (Fig. 7) at 300 s (■) and 3600 s (●) as a function of polarization potential. (b) Integrated charges passed in potentiostatic transients as a function of polarization potential at the C-cloth electrode; comparison of charges evaluated at 300 s (■) and 3600 s (●).

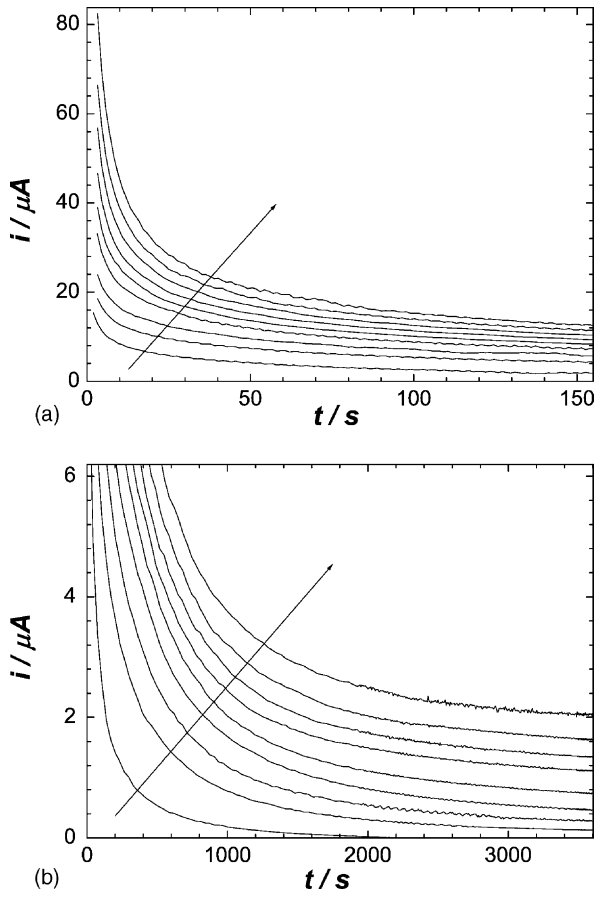

Fig. 9. As in Fig. 7, but for float-currents measured in 5.0 M H_2SO_4 at a glassy-C electrode to 150 and 3600 s. Arrows show directions of increasing initial anodic polarization potentials.

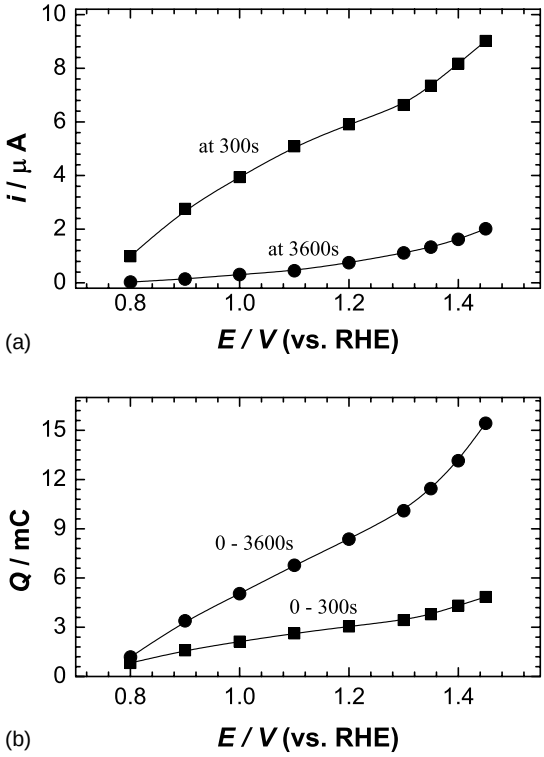

Fig. 10. (a) Response current values during the transients (Fig. 9) for the glassy-C electrode as a function of polarization potential, recorded at times $t = 300$ s (■) and 3600 s (●). (b) Integrated charges passed in potentiostatic transients as a function of polarization potential at the glassy-C electrode; comparison of charges evaluated at 300 s (■) and 3600 s (●).

into the electrode, following the potential step. Examples are shown in Fig. 8, derived from the experimental transients of Fig. 7, evaluated at $t = 300$ and 3600 s in the transient.

The duration of the potentiostatic transients (on the order of several hundreds of seconds) is seen to be much larger than it would be for potential step experiments at plane electrodes, where it is on the order of μs to ms, e.g. Ref. [14]. This is, of course, due both to the very much larger and distributed nature of the capacitance of porous-C electrodes than that of plane electrodes of the same element, e.g. as for glassy-C (Figs. 5 and 9, and Section 9 below).

9. Comparative float-current behavior at glassy-carbon

Self-discharge float-current measurements were made comparatively at glassy-C, a much less porous material than the C-cloth. Fig. 9 shows the adjustment of float-current, i, following potentiostatic polarization to a series of potentials, E, over the range 1.45–0.8 V (RHE) taken at 50–100 mV intervals, recorded over 3600 s. The true float-currents are those towards the end of the transients (>1000 s) in Fig. 9. Resulting plots of i as a function of E are shown in Fig. 10a taken at 300 and 3600 s; as expected, the float-currents required to balance self-discharge rates increase with E (3600 s values). At 300 s, charging of C in the potentiostatic steps takes the principal current due to the bifurcation at A in Circuit 2. The integrated charges accumulated in the transients are plotted in Fig. 10b for $t = 300$ and 3600 s as $f(E)$. Note that the charges passed and the float-current magnitudes of the transients are much less than those for the porous, high-area C-cloth electrodes (Fig. 8), as is to be expected.

10. Analysis of float-current behavior of a capacitor under potentiostatic conditions

The most direct way to examine self-discharge of a capacitor by the "float-current" method is to apply potentiostatic polarization steps to a series of electrode potentials at which self-discharge rates are to be evaluated, and then record the resulting currents, as indicated earlier.

In the absence of self-discharge, the charging situation can be usefully represented by a "first-order" (cf. Ref. [1]) equivalent circuit having the form:

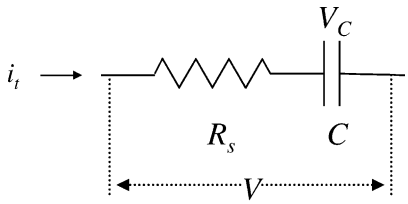

Circuit 1

in which charging current, i_t, enters through an (equivalent) series resistance, R_S, into the capacitance, C. During passage of charge due to application of a constant V, the latter potential difference, V, becomes distributed across Circuit 1 as

$$V = i_t R_S + V_C \tag{7}$$

where V_C is the time-dependent potential across the capacitor, $= V - i_t R_S$. The time-dependent charging-current, i_t, is then

$$i_t = C\frac{d(V - i_t R_S)}{dt} \tag{8}$$

$$= -CR_S\frac{di_t}{dt} \tag{9}$$

for constant applied V, i.e., upon integration:

$$i_t = i_i \exp\left[-\frac{t}{R_S C}\right] \tag{10}$$

where i_i is the initial current at $t \to 0$. Hence the charging current exponentially decreases in time t.

Note that, in a *porous electrode*, the R_S (determining rates of admission of charge to the outer surface of the capacitor electrode), is coupled with the distributed resistance and capacitance, in the carbon electrode matrix which is therefore microscopically being charged at a distribution of rates (de Levie porous-electrode effect [13]). The effective "R" is then a combination of R_S and distributed resistance in the porous matrix. An experimental demonstration of this, more complex situation, was made by means of a five-element hardware circuit in the paper of Ref. [15], published earlier from our laboratory. Using that model it was possible to record the time dependence of potentials at each C–R connection point in the five-element C/R ladder.

The situation obtaining when C is subject to self-discharge, characterized by a potential-dependent resistance R_{SD}, is represented simplistically by the "first-order" (cf. Refs. [11,12]) series/parallel circuit shown below:

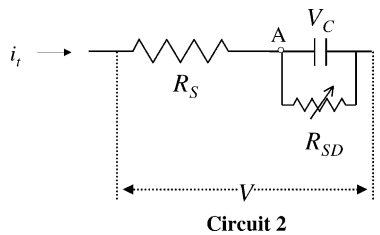

Circuit 2

where the possibility that R_{SD} is potential-dependent is indicated. Then potentiostatic charging (V = constant) results in a bifurcation of current at A into two components: i_C the charging current into C and the self-discharge current, i_{SD}, related to V_C and R_{SD} at a given state of charge of C, the latter determining V_C in Circuit 2. Note that as V_C builds up, the i_{SD}, through R_{SD}, tends to increase.

Then two limiting cases arise: (a) when $R_{SD} \gg R_S$ (very slow self-discharge) almost normal charging of C (with rise of V_C) will arise according to Eq. (10) with $R \approx R_S$; (b) when $R_{SD} \ll R_S$, most of the current passes through R_{SD}, corresponding to high self-discharge rate, i.e. an high float-current would be required to maintain charge on C. See results of simulation calculations in Section 11, below. A more complex situation arises when R_{SD} is itself potential-dependent as for a Faradaic leakage process. This case will be treated elsewhere.

Practically, an intermediate situation will normally arise, dependent on the value of V, where, in the charging transient, part of the current goes for charging C and a parasitic fraction passes through R_{SD}. In the steady state, it is the latter that is measurable as the float-current, and the state-of-charge of C is less than that attainable (for a given V) where self-discharge is negligible.

The above situations provide a primitive basis for understanding of the results shown above, obtained by potentiostatic-step experiments with the porous C-cloth electrode. In Fig. 7 was shown the charging-current transients for the C-cloth electrode recorded for five constant potentials from 1.1 to 0.8 V (RHE).

11. Simulation of the float-current behavior modeled in circuit 2

Although for a variety of applications, electrochemical capacitors having small capacities operate with charge/discharge time-scales of ms to several seconds, so that extents of self-discharge are correspondingly quite small, larger asymmetric cell devices are designed to operate over charge/discharge cycles of several hours, i.e. comparable with times over which appreciable self-discharge can take place. This is the case treated in this section of the paper.

In the following the purpose is hence to demonstrate how, in a potentiostatic float-current transient, the current arising from a potential step (V) becomes bifurcated at A in Circuit 2 into two components, one for charging of the capacitance, the other passing in parallel as a self-discharge (SD) current. The values of these components depend on the relative values of R_S and R_{SD} (the resistance equivalent to the reciprocal rate of the self-discharge process at some given electrode potential). Naturally, the smaller is R_{SD} compared with the ESR, R_S, the greater will be the self-discharge rate and thus the float-current *required* to maintain the given potential. As a consequence, the SOC of the capacitance, C, at a given potential remains lower than that for the larger R_{SD} and the behavior depends, in fact, on the ratio of R_{SD} to R_S.

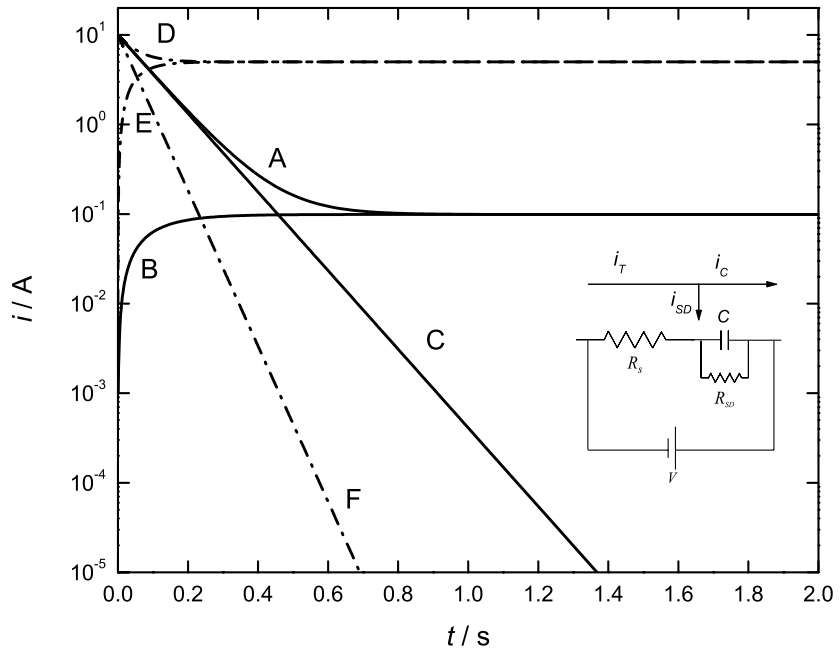

Fig. 11. Calculated float-current transients, plotted on $\log i$ vs. t-scale, obtained when C is subject to self-discharge through a constant resistance, R_{SD}, as represented by the series/parallel RC Circuit 2 (Section 10): $C = 1\,F$; $V = 1\,V$; $R_S = 0.1\,\Omega$. For $R_{SD}/R_S = 1$, the total current, i_T, is plotted as curve A; the self-discharge current, i_{SD}, is plotted as curve B and the capacitor charging current, i_C, is plotted as curve C. For $R_{SD}/R_S = 100$, i_T is curve D, i_{SD} is curve E and i_C is curve F.

This situation is illustrated in Figs. 11 and 12 by quantitative simulations of the charging and float-current behaviors. In Fig. 11 the total, the $i_T(t)$, self-discharge, $i_{SD}(t)$, and the capacitor charging currents, $i_C(t)$, are plotted as a function of time for a nominal voltage of 1 V, applied to a capacitance C of 1 F for two different examples having constant ratio of R_{SD}/R_S of 100 and 1. Plotted in curves A, B and C are $i_T(t)$, $i_{SD}(t)$ and $i_C(t)$, respectively, for the case in which R_S and R_{SD} are taken as nominally equal (i.e. $R_{SD}/R_S = 1$). Such conditions actually correspond to an unrealistic situation in which the capacitor element is subject to considerable self-discharge, e.g. as at elevated temperatures. Plotted as curves D, E and F are $i_T(t)$, $i_{SD}(t)$ and $i_C(t)$, respectively, for the case in which R_{SD} is two orders of magnitude larger than R_S (i.e. $R_{SD}/R_S = 100$, relatively lower self-discharge rate). For simplicity of calculation, unlike in Circuit 2, R_{SD} is assumed to be potential-independent. For the case of constant (potential-independent) self-discharge resistance, the charging current across the capacitor, i_C, is a function of both R_S and R_{SD},

$$i_C(t) = \frac{V}{R_S} \exp\left[-\frac{1 + (R_S/R_{SD})}{R_S C} t\right] \tag{11}$$

The capacitor voltage profile is also a function of t and is

$$V_C(t) = \frac{R_{SD} V}{R_S + R_{SD}} \left(1 - \exp\left[-\frac{1 + (R_S/R_{SD})}{R_S C} t\right]\right) = i_{SD} R_{SD} \tag{12}$$

Clearly the log of the capacitor charging current is linear in t (Eq. (11), curves C and F of Fig. 11); however, the total and self-discharge currents are not (see Fig. 11; curves A, D and B, F are for $i_T(t)$ and $i_{SD}(t)$, respectively, and also Eq. (12) given that $i_{SD} = V_C(t)/R_{SD}$). The self-discharge current is then a function of the form $A[1 - \exp(-Bt)]$. The total cumulative charges delivered, the cumulative charge at the capacitor and the capacitor voltage (V_C) are each dependent both on the ratio of R_{SD}/R_S and on time as clearly shown in Fig. 12. For a given R_S, decreasing the ratio R_{SD}/R_S results in a relative increase in the self-discharge current and, therefore, a decrease in both the cumulative charge stored

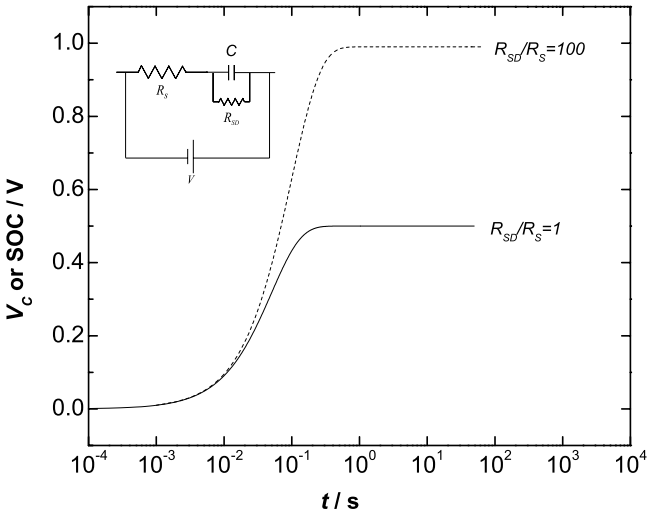

Fig. 12. As for Fig. 11, but for calculated capacitor voltage, V_C, as a $f(t)$: (—) $R_{SD}/R_S = 1$; (- - -) $R_{SD}/R_S = 100$.

and the voltage V_C across the capacitor. These simulation calculations give a useful overall view of the dynamics of float-current measurements and hence of their significance in time.

12. "One-electrode" versus "two-electrode" measurements

Often, in technical evaluations of power-source performance, two-terminal open-circuit self-discharge rates are recorded for practical purposes. However, such measurements give no indication of which electrode (positive or negative) is contributing mainly to the self-discharge, or, if both are, to comparable extents. This is of major importance in the newer, asymmetric (or so-called hybrid) electrode configurations of electrochemical capacitors [16] where the capacitor electrode usually suffers faster self-discharge than the battery-type electrode component in an asymmetric device. This situation is illustrated in Fig. 6.

If such a situation arises, subsequent recharge will cause overcharge on the electrode that has suffered less discharge than the other, unless interim, slow short-circuit completion of discharge has been carried out (an undesirable and complicated experiment).

Hence it is very desirable that information on self-discharge rates be obtained *individually on each electrode*. This can be done in separate experiments on each electrode (in a cell with a third electrode as a reference) or in a two-electrode device cell in which a wick or capillary electrolyte probe contact is made into the cell from a (third) electrode as reference, through its top, contacting the separator. This procedure has been used in our lab for some time and its effectiveness proven. An example is shown in Fig. 13 for self-discharge at the electrodes of an asymmetric cell comprised of a C double-layer anode and a PbO_2 cathode [17].

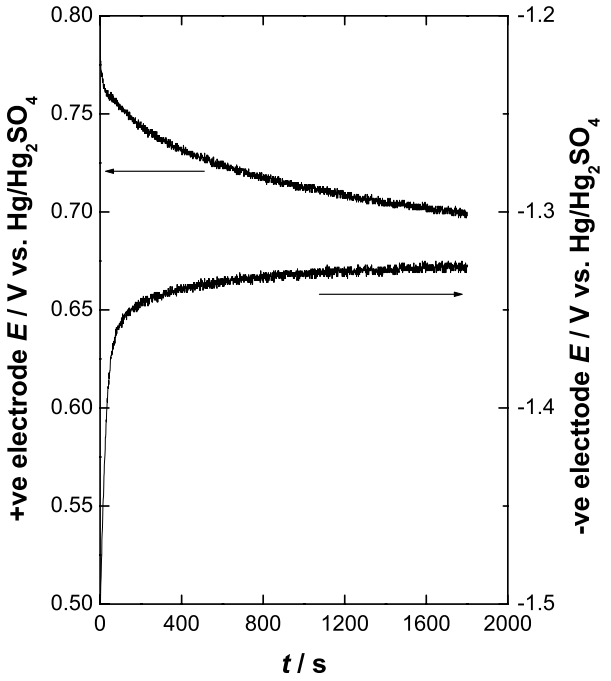

Fig. 13. Illustrating asymmetry of self-discharge between the positive and negative electrodes of an electrochemical capacitor, especially for the "hybrid" type comparing a C (negative) double-layer-type electrode worked against a Pb/PbO_2 (positive) Faradaic battery-type electrode.

From results of such tests, some adjustments of mass (≡charge capacities) of the conjugate positive and negative electrodes can be made to minimize the effects of asymmetric self-discharge rates. This, however, may not be easy since mass and charge capacities must also be balanced complementarily in terms of relative equivalent weight of the positive and negative electrodes required for optimized charge and discharge cycling [17]. This factor is especially important for the "hybrid electrode" systems (e.g. Refs. [16,17]) where, e.g., a $PbO_2/PbSO_4$ positive electrode is operated down to not more than 60% state of discharge to preserve long cyclability and optimization of rate capability.

13. Conclusions

1. Self-discharge behavior at porous-C double-layer capacitor electrodes differs in important ways from that at battery-type electrodes, e.g. Ni–O–OH.
2. Plots of potentials on self-discharge both at the C-cloth electrode and a glassy-C electrode are logarithmic in time but exhibit different slopes, $dE/d(\log t)$ or $dE/d(\log(t+\theta))$, depending on the initial polarization potentials (in contrast to behavior of Ni–O–OH).
3. Float-current measurements of self-discharge rates are complementary to data obtained from potential-decay behavior in time. They have been conducted at the C-cloth and glassy-C electrodes. Interpretation of the resulting data is, however, complicated at high-area porous electrodes by time-dependent processes over 100s to 1000s of seconds due to *t*-dependent charging in parallel with ultimate matching of the SD balanced charging rate.
4. Analysis of behavior of equivalent circuits to model float-current behavior at porous carbon electrodes gives useful bases for interpretations of the experimental results.
5. Stress is put on the desirability of characterizing SD at *individual* electrodes in cell-pairs by recording time-dependent potentials or float-currents versus the potential of a "third-electrode" as a reference having access to the cell.
6. This procedure is of particular value with asymmetric-type electrode configurations where SD behavior can be quite different at the Faradaic electrode from that at the non-Faradaic (capacitative) one, giving rise to asymmetric SD in the cell.

Acknowledgements

Grateful acknowledgement is made to the Natural Sciences and Engineering Research Council of Canada for support of this work on a Strategic Research Grant. Thanks are due to Dr. N. Marincic for the opportunity of verbally presenting this paper at the 13th International Symposium on Double-layer Capacitor and Related Hybrid Devices (Deerfield Beach, FL, December 2003).

References

[1] W.G. Pell, B.E. Conway, in: Proceedings of the Sixth International Seminar on Double-Layer Capacitor and Similar Devices, Deerfield Beach, FL, Florida Educ. Seminars Inc., Boca Raton, FL, 1996.
[2] B.E. Conway, J. Electrochem. Soc. 138 (1991) 1539.
[3] B.E. Conway, Electrochemical Supercapacitors: Scientific Principles and Technological Applications, Kluwer Academic Publishers–Plenum Press, New York, 1999.
[4] B.E. Conway, J. Electrochem. Soc. 138 (1991) 1539.
[5] A.D. Burke, in: Proceedings of the Third International Seminar on Double-Layer Capacitors and Similar Devices, Deerfield Beach, FL, Florida Educ. Seminars Inc., Boca Raton, FL, 1993.
[6] D.C. Grahame, Chem. Rev. 41 (1947) 441.
[7] W.G. Pell, B.E. Conway, J. Electroanal. Chem. 500 (2001) 121.
[8] B.E. Conway, P.L. Bourgault, Can. J. Chem. 40 (1962) 1690, 1938.
[9] B.E. Conway, E. Gileadi, Trans. Faraday Soc. 58 (1962) 2493.
[10] J.R. Miller, Electrochem. Soc. Proc. 29–95 (1995) 246.
[11] R.A. Dougal, L. Gao, S. Liu, J. Power Sources 126 (2004) 250.
[12] J.R. Miller, S.M. Butler, in: Proceedings of the Electrochemical Society Symposium on Electrochemical Capacitor and Hybrid Power Sources, vol. 7, The Electrochemical Society Inc., 2002, p. 28.
[13] R. de Levie, Electrochim. Acta 8 (1963) 751.
[14] A.J. Bard, L.R. Faulkner, Electrochemical Methods, Wiley, New York, 1980, Chapter 5, p. 136.
[15] W.G. Pell, B.E. Conway, W.A. Adams, J. de Oliveira, J. Power Sources 80 (1999) 134.
[16] Proceedings of the Electrochemical Society Symposium on Electrochemical Capacitor and Hybrid Power Sources, vol. 7, The Electrochemical Society Inc., 2002.
[17] W.G. Pell, B.E. Conway, J. Power Sources, in press.